

# Response of the low-level jet to precession and its implications for proxies of the Indian monsoon

Chetankumar Jalihal<sup>1</sup>, Jayaraman Srinivasan<sup>2</sup>, and Arindam Chakraborty<sup>2</sup>

<sup>1</sup>Indian Institute of Science Bangalore

<sup>2</sup>Indian Institute of Science

November 23, 2022

## Abstract

The long-term variations in the South Asian monsoon have been inferred based on the variations in the ocean productivity along the western coast of the Arabian Sea. The variations in ocean productivity were previously thought to be primarily influenced by the intensity of upwelling. Here, using idealized precession experiments in fully coupled climate models, we have shown that the area as well as the region of maximum upwelling change with precession. When summer occurs at perihelion (stronger summer insolation and monsoon precipitation) the area of upwelling is narrow. In contrast, during summer at aphelion (weaker summer insolation and monsoon precipitation), upwelling occurs over a broader region. This is due to the effect of convective heating over northeastern Africa and the western equatorial Indian ocean on the width and meridional location of the low-level jet. Therefore, the upwelling inferred from proxies does not necessarily indicate the Indian summer monsoon strength.

# Response of the low-level jet to precession and its implications for proxies of the Indian monsoon

Chetankumar Jaliha<sup>1,2\*</sup>, Jayaraman Srinivasan<sup>2</sup>, Arindam Chakraborty<sup>1,2</sup>

<sup>1</sup>Centre for Atmospheric and Oceanic Sciences, Indian Institute of Science, Bangalore, 560012, India

<sup>2</sup>DST-Centre of Excellence in Climate Change, Divecha Centre for Climate Change, Indian Institute of Science, Bangalore, 560012, India

## Key Points:

- Upwelling in the Arabian Sea in modern climate is closely linked to the strength of the low-level jet and the South Asian summer monsoon.
- On longer timescales, along with the strength of the jet, the location as well as the width of the jet change.
- This affects the intensity and spatial extent of upwelling and has implications for the interpretation of proxies of upwelling.

---

\*Max Planck Institute for Meteorology, Hamburg 20146, Germany

Corresponding author: Chetankumar Jaliha, [jaliha@iisc.ac.in](mailto:jaliha@iisc.ac.in)

**Abstract**

The long-term variations in the South Asian monsoon have been inferred based on the variations in the ocean productivity along the western coast of the Arabian Sea. The variations in ocean productivity were previously thought to be primarily influenced by the intensity of upwelling. Here, using idealized precession experiments in fully coupled climate models, we have shown that the area as well as the region of maximum upwelling change with precession. When summer occurs at perihelion (stronger summer insolation and monsoon precipitation) the area of upwelling is narrow. In contrast, during summer at aphelion (weaker summer insolation and monsoon precipitation), upwelling occurs over a broader region. This is due to the effect of convective heating over northeastern Africa and the western equatorial Indian ocean on the width and meridional location of the low-level jet. Therefore, the upwelling inferred from proxies does not necessarily indicate the Indian summer monsoon strength.

**Plain Language Summary**

Modern observations suggest that the upwelling along the eastern coast of the Arabian Sea is primarily controlled by the strength of the low-level jet (LLJ). The strength of the LLJ and the Indian summer monsoon rainfall are also positively correlated. Hence, proxies of upwelling have been used to infer the variations in the monsoon of the distant past. We find, however, that factors other than the strength of the LLJ also affect upwelling. Variations in Earth's orbit alter the latitudinal location and width of the LLJ. This affects the area over which upwelling occurs and shifts the region of maximum upwelling. During periods of weaker summer insolation, the LLJ is broader and further south. This leads to an increase in the spatial extent of the upwelling. Therefore, the ocean productivity in the Arabian Sea is higher during such periods. This explains the large lag ( $\sim 9$  kyrs) with respect to the local summer insolation as observed in these proxies. Thus, we conclude that the proxies of upwelling capture multiple signals resulting from changes in the location, width, and strength of the LLJ and hence are not appropriate for deducing the long-term variations in monsoon rainfall.

**1 Introduction**

The low-level jet (LLJ) in the Arabian Sea is a prominent feature of the Indian summer monsoon (Findlater, 1969, 1974; Halpern & Woiceshyn, 2001; Rajendran et al., 2012). The jet carries moisture from the Indian Ocean onto the Indian subcontinent. Thus, the strength of the LLJ is positively correlated with the Indian summer monsoon rainfall in the modern climate (Joseph & Sijikumar, 2004; Chakraborty et al., 2002, 2009). The coastal upwelling induced by the LLJ is proportional to the strength of the LLJ, and therefore, stronger monsoons produce larger upwelling (Murtugudde et al., 2007). This relation has been used to reconstruct the strength of the past monsoons. Regions of upwelling are also regions of higher ocean productivity. Therefore, by measuring the productivity in these regions as archived in the sediment cores, upwelling can be inferred.

Evidence from such reconstructions indicates that the strength of upwelling lags local summer insolation by about 9 kyrs (S. Clemens et al., 1991; Reichert et al., 1998; S. C. Clemens & Prell, 2003; S. C. Clemens et al., 2010; Caley et al., 2011). Whether this can be interpreted as a lag in the South Asian monsoon has been a subject of debate (Gebregiorgis et al., 2020; Zhang et al., 2020) because terrestrial proxies of monsoon suggest that monsoon rainfall is nearly in phase with local insolation (Zhang et al., 2019). Therefore, the proxies of upwelling in the Arabian Sea are thought to represent the strength of the LLJ instead (Gupta et al., 2005). Thus, indicating that the relationship between LLJ and the monsoon rainfall may be different in different climate regimes. This view is supported by recent studies where it was shown that it is the net energy flux into the atmosphere and water vapor, and not the monsoon winds that account for vari-

ability of South Asian monsoon on centennial and longer timescales (Jalihal, Srinivasan, & Chakraborty, 2019; Jalihal et al., 2020).

The variations in precipitation over the Bay of Bengal are, however, linked to those in LLJ on precession timescales (Jalihal, Bosmans, et al., 2019; Jalihal et al., 2020). The LLJ extends into the Bay of Bengal and modulates the surface latent heat flux there. These fluctuations in the surface latent heat flux are large enough to counter the changes induced by insolation. Hence, precipitation over the Bay of Bengal is out-of-phase with local summer insolation. This has also been documented in proxy reconstructions (Gebregiorgis et al., 2018; McGrath et al., 2021), and it has been found to be consistent with the proxies of upwelling in the Arabian Sea (Gebregiorgis et al., 2018). Thus, the orbital-scale variations in LLJ is linked to oceanic precipitation and not to the terrestrial precipitation within the South Asian monsoon domain.

The variations in the LLJ on intraseasonal and interannual timescales has been studied extensively (Chen & van Loon, 1987; Arpe et al., 1998; Halpern & Woiceshyn, 2001; Fasullo & Webster, 2002; Joseph & Sijikumar, 2004; Jain et al., 2021). Several studies have also highlighted that LLJ location and intensity are changing and are likely to change further due to global warming (Rajendran et al., 2012; Sandeep & Ajayamohan, 2015; Decastro et al., 2016; Preethi et al., 2017; Sandeep et al., 2018). A comprehensive study of LLJ variations on the orbital timescale is, however, missing. An understanding of the long-term variations in LLJ and the factors that drive it is necessary for the correct interpretation of the proxies. In this article, using fully coupled general circulations models, we have unraveled the factors that affect upwelling on the orbital timescale.

## 2 Data and Methods

We have used NCEP reanalysis over the period 1948–2017 to understand the connection between upwelling and precipitation at the interannual timescales. Upwelling is calculated based on the curl of windstress. GPCP monthly precipitation data is used to evaluate precipitation over India. Reconstructions of upwelling from the Arabian Sea give an estimate of the upwelling on longer timescales. We have used several foraminifer assemblages from the cores RC27-61 (S. C. Clemens & Prell, 2003), MD04-2861 (Caley et al., 2011), and GeoB3004-1 (Schmiedl & Leuschner, 2005). The productivity estimates from the NIOF cores 455, 464, and 497 (Reichart et al., 1998) were also used. Furthermore, denitrification in the oxygen minimum zone also represents upwelling (Reichart et al., 1998; Altabet et al., 2002). Hence, we have used  $\delta^{15}\text{N}$  from the cores RC27-14 and RC27-23 (Altabet et al., 2002). These are compared with the  $\delta^{18}\text{O}_{\text{sw}}$  ( $\delta^{18}\text{O}$  of seawater; see methods in Jalihal, Srinivasan, and Chakraborty (2019) for a detailed description) from a sediment core near the mouth of Ganga-Brahmaputra in the northern part of the Bay of Bengal (Kudrass et al., 2001). Since this region is influenced by the runoff from over land, this proxy captures the amount of terrestrial monsoon rainfall. All the proxies are interpolated to an equally spaced interval of 500 years, following which a bandpass filter is applied to extract the precession modes (18 - 24 kyrs).

We have carried out time slice orbital experiments in the high resolution, fully coupled CESM 1.2.0 (Neale et al., 2010; Hurrell et al., 2013). The model consists of the CAM 5 (Community Atmospheric Model) for the atmospheric component and Parallel Ocean Program (POP) for the ocean model. CAM has a resolution of  $0.9^\circ \times 1.2^\circ$ , whereas the POP has a resolution of about  $0.25^\circ$  near the equator. The model was run with orbital configurations corresponding to the minimum and maximum precession ( $P_{\text{min}}$  and  $P_{\text{max}}$ ), following the experimental setup used by Bosmans et al. (2015). In the precession minimum ( $P_{\text{min}}$ ) orbital configuration, the boreal summer solstice occurs near the perihelion, whereas in the Precession maximum ( $P_{\text{max}}$ ), it occurs at aphelion. The eccentricity is set close to the highest values that occurred in the last million years. This produces a difference in summer insolation (Jun-Jul-Aug) between  $P_{\text{min}}$  and  $P_{\text{max}}$ , over India of

about 80 Wm<sup>-2</sup> (Berger, 1978; Bosmans et al., 2015, 2018; Jaliha, Bosmans, et al., 2019). Each simulation is run for 100 years. The first 50 years of the simulation are discarded as spin-up, and only the last 50 years are considered for the study. All the other boundary conditions are kept constant at their pre-industrial values. The model has a decent representation of the climatological Indian summer monsoon and reproduces the seasonal cycle quite well (Supplementary figures 1 and 2). To validate our results, we have used data from the P<sub>min</sub> and P<sub>max</sub> simulations from another high-resolution model: EC-Earth (Bosmans et al., 2015).

The Ekman upwelling was evaluated as the curl of wind stress over the surface of the ocean:

$$W_e = \text{curl} \left( \frac{\tau}{\rho f} \right) \quad (1)$$

Where,  $W_e$  is the upwelling averaged over the Ekman layer,  $\rho$  is the density of sea water (taken to be 1025 kg m<sup>-3</sup>),  $f$  is the Coriolis parameter,  $\tau$  is the wind stress on the surface of the ocean.  $\tau$  is given by:

$$\tau = \rho_a * C_d * W S_{sfc} \quad (2)$$

$\rho_a$  is the density of air (taken to be 1 kg m<sup>-3</sup>),  $W S_{sfc}$  is the surface wind speed (10 m wind speed is used from NCEP and wind speed at 0.995 sigma for model data).  $C_d$  is the drag coefficient and is given by Large and Pond (1981):

$$C_d = 0.0013 \quad W S_{sfc} \leq 11 \text{ m s}^{-1} \quad (3)$$

$$C_d = 10^{-3}(0.49 + 0.065 * W S_{sfc}) \quad W S_{sfc} > 11 \text{ m s}^{-1} \quad (4)$$

### 3 Results

#### 3.1 Impact of precession on the relation between the Arabian Sea upwelling and South Asian monsoon

Fig. 1 depicts the correlation between the Indian summer monsoon rainfall (ISMR) and upwelling in the surrounding oceans at interannual timescales based on NCEP data. It shows that ISMR is positively correlated with upwelling in the northwestern Arabian Sea along the coast. At the precession mode, the reconstructions of upwelling within this region are, however, negatively correlated with the proxies of the Indian monsoon. This correlation is not spatially uniform. There are differences in the correlation as we move north. Near the horn of Africa, it is positively correlated, but changes sign further north. Thus, suggesting a complex relation between ISMR and upwelling on precession timescales ( $\sim 23$  kyrs).

Orbital forcing modulates both the ISMR as well as the LLJ (Jaliha, Bosmans, et al., 2019; McGrath et al., 2021). Therefore, we have examined the relation between ISMR and upwelling due to variations in Earth's orbit (Fig. 2). We find that the relation between ISMR and upwelling is different under different climates (Fig. 2). During periods of high local summer insolation and climatological monsoon (P<sub>min</sub>), the correlation between interannual variations in ISMR and upwelling is negligible. In contrast, during periods of weaker summer insolation and climatological monsoon (P<sub>max</sub>), the correlation between interannual variations in ISMR and upwelling is stronger. Thus, underscoring that the relationship between ISMR and upwelling as seen in modern observations should not be extended for all climates.

The orbital configuration of P<sub>max</sub> resembles the modern orbital configuration, albeit with higher eccentricity. The pattern of the correlation between ISMR and upwelling

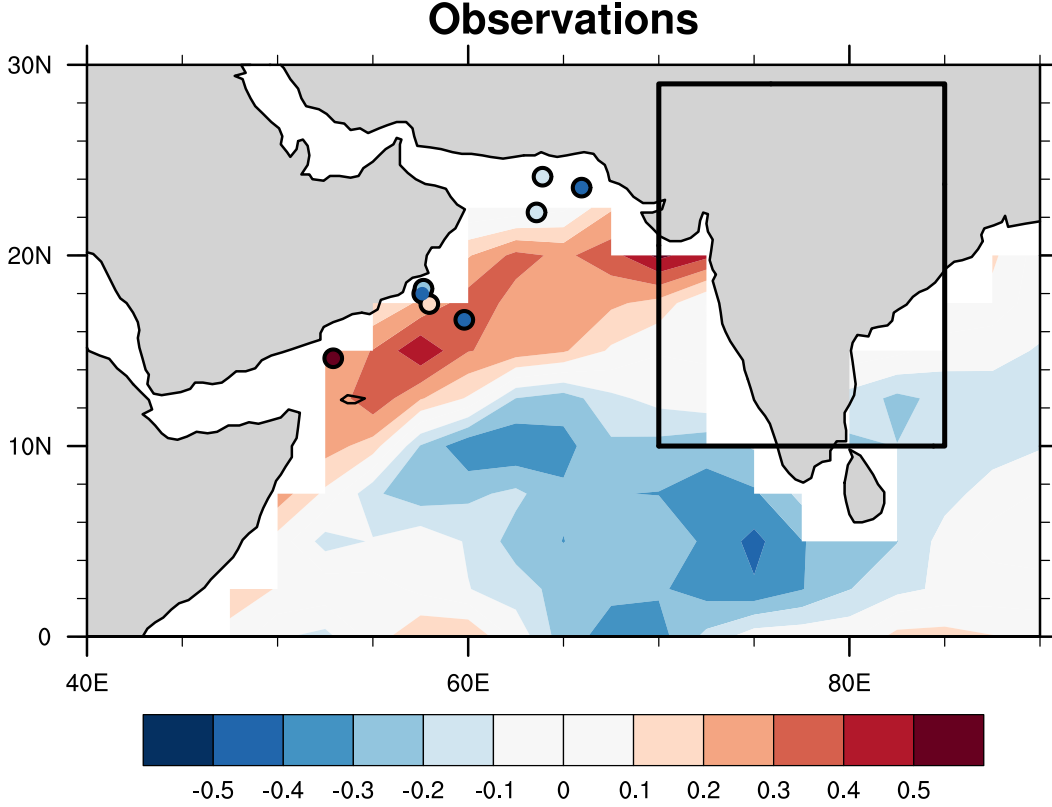


**Figure 1.** The spatial map of correlation between Jun-Jul-Aug (JJA) averaged rainfall over India and Ekman upwelling everywhere. The inset black box represents the region over which area-averaged precipitation was evaluated (10-29N; 70-85E; land only grids). NCEP-reanalysis 1 dataset was used to evaluate the curl of wind stress, and Global Precipitation Climatology Project (GPCP) dataset was used for precipitation. The filled circles show the correlation between the proxy of the Indian monsoon,  $\delta^{18}\text{O}_{\text{sw}}$  (Kudrass et al., 2001), with the proxies of upwelling in the Arabian Sea (Reichart et al., 1998; Altabet et al., 2002; S. C. Clemens & Prell, 2003; Schmiedl & Leuschner, 2005; Caley et al., 2011). These proxies were bandpass filtered for the precession modes (18–24 kyrs). The filled circles represent the location of the upwelling proxies. The color with which the circles are filled corresponds to the correlation of the proxy with that of the Indian monsoon proxy.

is, also, the same (Fig. 1 & Fig. 2b). The interannual variations in the latitude and strength of the LLJ is related to those in the gradient of surface pressure over the Arabian Sea (Tomas & Webster, 1997; Webster et al., 2003; Sandeep & Ajayamohan, 2015; Chakraborty & Agrawal, 2017). At the precession timescales, additional factors influence the location and strength of the LLJ (Jalihal, Bosmans, et al., 2019). Precipitation over northeastern Africa and the west equatorial Indian Ocean increase on account of higher summer insolation in  $P_{\text{min}}$  compared to  $P_{\text{max}}$ . The convective heating over these two regions drives a Matsuno-Gill-like response of the lower tropospheric winds (Jalihal, Bosmans, et al., 2019; Pausata et al., 2021). The ensuing Kelvin wave produces an anomalous easterly that leads to narrowing of the LLJ and also causes its maxima to shift northward (Jalihal, Bosmans, et al., 2019; Pausata et al., 2021). In the current study, we find a similar dependence at the interannual timescales as well in  $P_{\text{min}}$ . The interannual variations in precipitation over northeastern Africa and the west equatorial Indian Ocean have a greater impact on the LLJ, and hence on the upwelling in  $P_{\text{min}}$  (Supplementary Fig. 3a). In  $P_{\text{max}}$ ,

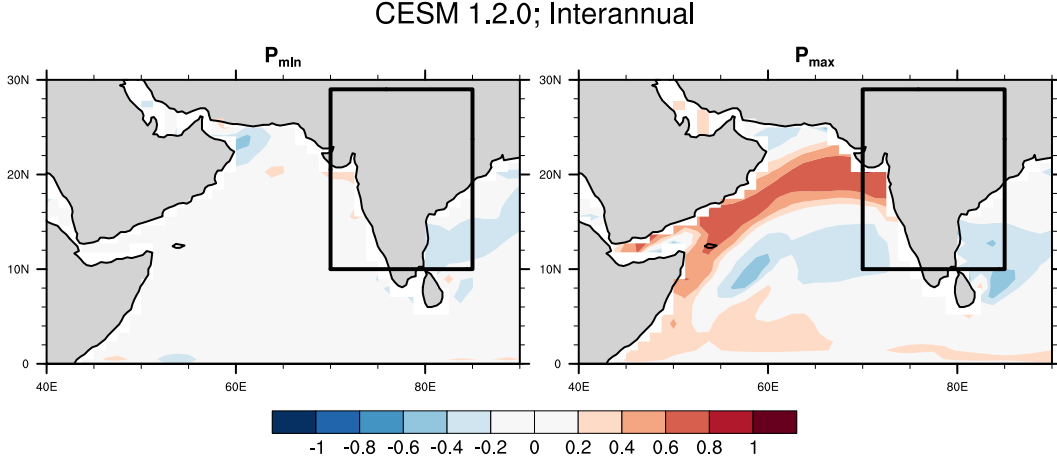


**Figure 2.** The spatial map of correlation between the Jun-Jul-Aug (JJA) mean Indian monsoon rainfall (Precipitation over the domain  $10^{\circ}$ - $29^{\circ}$ N;  $70^{\circ}$ - $85^{\circ}$ E; land only grids) with Ekman upwelling over grids everywhere. (a) is for the  $P_{\min}$  simulation, whereas, (b) is for the  $P_{\max}$  simulation. The last 50 years of the simulation were used to generate the correlation maps.

precipitation over these two regions is weaker. Therefore, they do not influence the upwelling in  $P_{\max}$  at the interannual timescales (Supplementary Fig. 3b).

### 3.2 Change in area of upwelling

The proxies used to detect upwelling, in general, record the integrated effect of several years. Therefore, we have examined the climatology in our simulations. A change in precession leads to meridional shifts in the LLJ (Fig. 3a&b). In  $P_{\min}$ , the LLJ is parallel to the coast of Oman and is located in the northern Arabian Sea. The climatological summer monsoon is stronger in this experiment. On the other hand, summer insolation and ISMR are weaker in  $P_{\max}$ . The LLJ is further south as compared to its location in  $P_{\min}$ . Along with this southward shift, the strength of the LLJ also changes. The maximum velocity is higher in  $P_{\max}$  and is located near the horn of Africa. There is a change in the width of the LLJ as well. The LLJ is broader in  $P_{\max}$  and is narrower in  $P_{\min}$  (Fig. 3 a & b). Thus, suggesting that the orbital scale variability of the LLJ consists of fluctuations in the strength, meridional location, and width, whereas, its interannual fluctuations are primarily due to changes in its strength (Supplementary figure 4). The variations in the strength, magnitude, and location of the LLJ on precession timescales are due to the additional influence of convective heating over northeastern Africa and the west equatorial Indian Ocean (Jalihal, Bosmans, et al., 2019; Pausata et al., 2021).

Since upwelling is determined by the curl of wind stress, any changes in the location, width, or strength of the LLJ would have an impact on upwelling. Therefore, we have compared the curl of wind stress from the two experiments to understand the impact of the changes in the LLJ (Fig. 4). In  $P_{\min}$  (stronger summer insolation), upwelling is concentrated along the eastern coast of the Arabian Sea and extends all the way into the northern parts of the Arabian Sea. In  $P_{\max}$ , the intensity of upwelling increases along the horn of Africa. The region of largest upwelling is, however, concentrated at  $15^{\circ}$ N. The upwelled water gets advected along with the nutrients to the northern Arabian Sea (Caley et al., 2011). Therefore, most of the proxies would capture a stronger signal in climates with  $P_{\max}$ -like orbital configurations. Furthermore, the area over which upwelling occurs in the northern Arabian Sea more than doubles in  $P_{\max}$ . This explains why most of the proxies suggest a large lag with respect to the local summer insolation. Such changes

**CESM 1.2.0; Climatology**

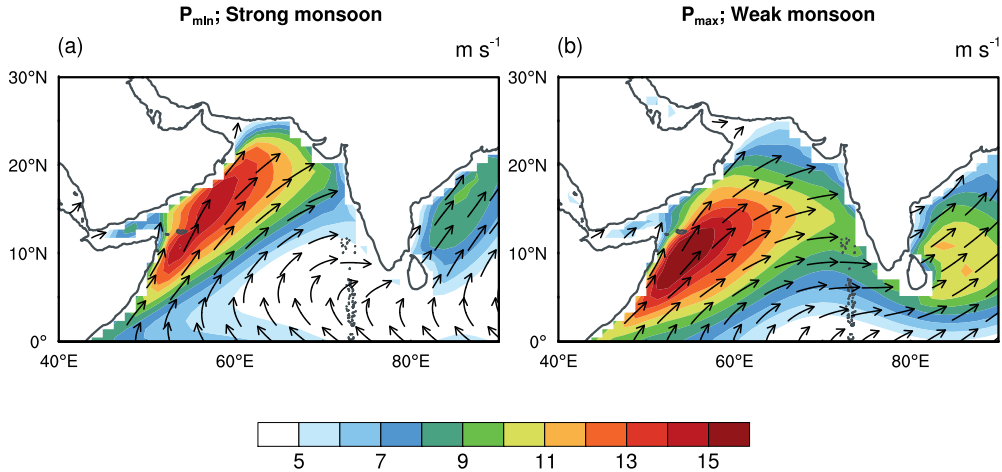


**Figure 3.** The Jun-Jul-Aug averaged climatological surface wind speed in shading for (a)  $P_{\min}$  (strong monsoon) and (b)  $P_{\max}$  (weak monsoon). The unit vectors indicate the direction of surface winds.

in the area of upwelling are not observed on interannual timescales (Supplementary Fig. 5). These results are consistent in  $P_{\min}$  and  $P_{\max}$  simulations using another fully coupled model- EC-Earth (Supplementary Fig. 6).

**CESM 1.2.0; Climatology**

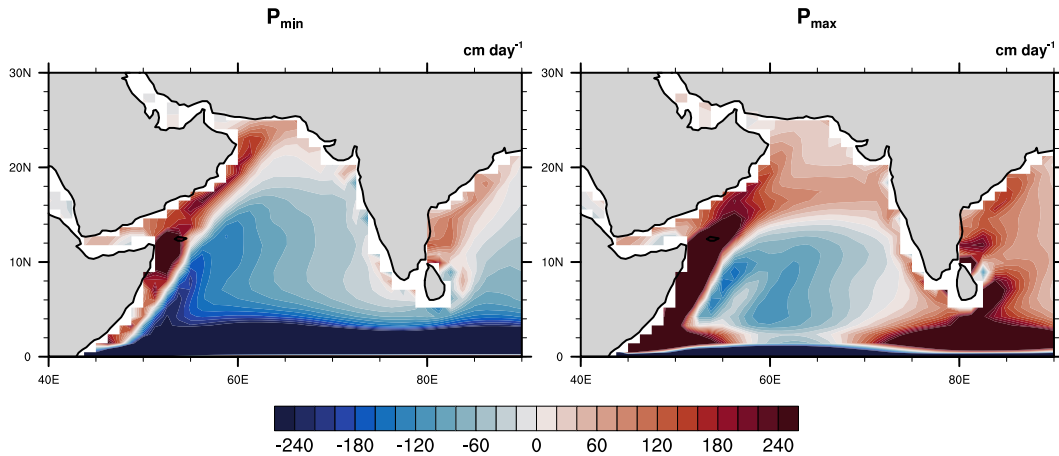


**Figure 4.** The Jun-Jul-Aug averaged climatological Ekman upwelling in shading for the climate for (a)  $P_{\min}$  (strong monsoon) and (b)  $P_{\max}$  (weak monsoon).

**4 Discussion and conclusions**

Terrestrial and marine reconstructions of the South Asian monsoon are inconsistent in terms of phase (Wang et al., 2014; Gebregiorgis et al., 2020; Cheng et al., 2021; McGrath et al., 2021). This is primarily due to the different responses of precipitation over land and ocean to changes in precession (Jalihal, Bosmans, et al., 2019). This phase

difference between India and the Bay of Bengal has been explored in detail (Battisti et al., 2014; Jalihal, Bosmans, et al., 2019; Jalihal et al., 2020). The connection between the precipitation over the Bay of Bengal and winds in the Arabian Sea were established both in the proxies (Gebregiorgis et al., 2018) and the models (Jalihal, Bosmans, et al., 2019). A comprehensive mechanism for the cause of lag in the proxies from the Arabian Sea was still missing. Furthermore, the differences in the sign of the correlation between the Indian monsoon rainfall and upwelling at interannual and precession modes were not explained in the previous studies.

In this study, we have demonstrated that along with the changes in wind speed of the low-level jet, the changes in the width of the jet, and its meridional location has an influence on upwelling in the Arabian Sea. On interannual timescales, the changes in the wind speed governs upwelling. At the precession timescales, the variations in the width and latitude of the jet also play a crucial role. These are influenced by convective heating in the west equatorial Indian Ocean and northeastern Africa (Jalihal, Srinivasan, & Chakraborty, 2019). These convective heat sources are a result of precessional forcing. The changes in the strength, width, and latitude of the low-level jet are such that the curl of wind stress is stronger during climates with weaker summer insolation. Moreover, the spatial extent of upwelling is substantially larger. Thus, proxies register enhanced productivity (upwelling) in such climates even though the summer monsoon is weaker. Two high-resolution fully coupled climate models show consistent results, further enhancing confidence in our results. Thus, upwelling-based proxies do not represent the variability of the South Asian monsoon at the precession mode. This also explains the large lag observed between upwelling and other terrestrial proxies of the monsoon. These proxies were previously thought to represent the South Asian monsoon and were found to have a large lag with respect to the terrestrial proxies, sparking-off a long-standing debate (Wang et al., 2014; Caley et al., 2011; Zhang et al., 2019; Gebregiorgis et al., 2020; Zhang et al., 2020). Our results show that upwelling-based proxies in the Arabian sea are not linked to Indian monsoon rainfall at precession timescales.

Proxy reconstructions are based on the relation between physical processes observed in the modern climate. Our results underscore that additional factors can impact the interpretation of some of the proxies on longer timescales. For example, since the region of upwelling expands and shrinks out-of-phase with the strength of the Indian monsoon on precession timescales, the upwelling signal captured by the proxy in many cases is out-of-phase with the Indian monsoon.

### Acknowledgments

The NCEP reanalysis data was obtained from <https://psl.noaa.gov/data/gridded/data.ncep.reanalysis.html>. The GPCP precipitation data is publicly available at <https://psl.noaa.gov/data/gridded/data.ncep.reanalysis.html>. The  $\delta^{18}\text{O}$  from the sediment core in North Bay of Bengal (Kudrass et al., 2001) was obtained from <https://doi.pangaea.de/10.1594/PANGAEA.735053>. Data from the cores RC27-14 and RC27-23 (Altabet et al., 2002) can be accessed from <https://www.ncdc.noaa.gov/paleo-search/study/2617>. The data from NIOP497, NIOP464, and NIOP455 cores (Reichart et al., 1998) is available from <https://www.ncdc.noaa.gov/paleo-search/study/2557>. The data from the core RC27-61 (S. C. Clemens & Prell, 2003) can be accessed from <https://www.ncdc.noaa.gov/paleo-search/study/5882>. We are thankful to T. Caley for providing the data from the core MD04-2861 (Caley et al., 2011). Data from the core GeoB3004-1 is available at <https://doi.pangaea.de/10.1594/PANGAEA.738202>. The EC-Earth data used here can be accessed from <https://zenodo.org/record/4912315#.YL91DCORpJ1>. The servers hosting our CESM simulation data at the institute have been turned off in accordance with the lockdown guidelines. Hence, as of now, we were not able to deposit the data in any repository. However, we confirm that the relevant data will be made available through a suitable data repository at the earliest possible.

We thank Supercomputer Education and Research Centre (SERC), Indian Institute of Science, Bangalore, for making available the computation facilities to carry out the simulations. The authors acknowledge support from the Centre for Excellence in the Divecha Centre for Climate Change (DCCC), supported by the Department of Science and Technology, Government of India. C.J. is grateful to DCCC for financial assistance.

## References

- Altabet, M. A., Higginson, M. J., & Murray, D. W. (2002). The effect of millennial-scale changes in arabian sea denitrification on atmospheric co<sub>2</sub>. *Nature*, *415*(6868), 159–162.
- Arpe, K., Dümenil, L., & Giorgetta, M. A. (1998). Variability of the indian monsoon in the echam3 model: Sensitivity to sea surface temperature, soil moisture, and the stratospheric quasi-biennial oscillation. *Journal of climate*, *11*(8), 1837–1858.
- Battisti, D., Ding, Q., & Roe, G. (2014). Coherent pan-asian climatic and isotopic response to orbital forcing of tropical insolation. *Journal of Geophysical Research: Atmospheres*, *119*(21), 11–997.
- Berger, A. (1978). Long-term variations of daily insolation and quaternary climatic changes. *Journal of Atmospheric Sciences*, *35*(12), 2362–2367.
- Bosmans, J., Drijfhout, S., Tuenter, E., Hilgen, F., & Lourens, L. (2015). Response of the north african summer monsoon to precession and obliquity forcings in the ec-earth gcm. *Climate dynamics*, *44*(1-2), 279–297.
- Bosmans, J., Erb, M., Dolan, A., Drijfhout, S., Tuenter, E., Hilgen, F., ... Lourens, L. (2018). Response of the asian summer monsoons to idealized precession and obliquity forcing in a set of gcms. *Quaternary Science Reviews*, *188*, 121–135.
- Caley, T., Malaizé, B., Zaragosi, S., Rossignol, L., Bourget, J., Eynaud, F., ... Ellouz-Zimmermann, N. (2011). New arabian sea records help decipher orbital timing of indo-asian monsoon. *Earth and Planetary Science Letters*, *308*(3-4), 433–444.
- Chakraborty, A., & Agrawal, S. (2017). Role of west asian surface pressure in summer monsoon onset over central india. *Environmental Research Letters*, *12*(7), 074002.
- Chakraborty, A., Nanjundiah, R., & Srinivasan, J. (2002). Role of asian and african orography in indian summer monsoon. *Geophysical research letters*, *29*(20), 50–1.
- Chakraborty, A., Nanjundiah, R. S., & Srinivasan, J. (2009). Impact of african orography and the indian summer monsoon on the low-level somali jet. *International Journal of Climatology: A Journal of the Royal Meteorological Society*, *29*(7), 983–992.
- Chen, T.-C., & van Loon, H. (1987). Interannual variation of the tropical easterly jet. *Monthly Weather Review*, *115*(8), 1739–1759.
- Cheng, H., Zhang, H., Cai, Y., Shi, Z., Yi, L., Deng, C., ... others (2021). Orbital-scale asian summer monsoon variations: Paradox and exploration. *Science China Earth Sciences*, 1–16.
- Clemens, S., Prell, W., Murray, D., Shimmield, G., & Weedon, G. (1991). Forcing mechanisms of the indian ocean monsoon. *Nature*, *353*(6346), 720–725.
- Clemens, S. C., & Prell, W. L. (2003). A 350,000 year summer-monsoon multi-proxy stack from the owen ridge, northern arabian sea. *Marine Geology*, *201*(1-3), 35–51.
- Clemens, S. C., Prell, W. L., & Sun, Y. (2010). Orbital-scale timing and mechanisms driving late pleistocene indo-asian summer monsoons: Reinterpreting cave speleothem  $\delta^{18}\text{O}$ . *Paleoceanography*, *25*(4).
- Decastro, M., Sousa, M., Santos, F., Dias, J., & Gómez-Gesteira, M. (2016). How will somali coastal upwelling evolve under future warming scenarios? *Scientific*

- reports*, 6(1), 1–9.
- Fasullo, J., & Webster, P. (2002). Hydrological signatures relating the asian summer monsoon and enso. *Journal of climate*, 15(21), 3082–3095.
- Findlater, J. (1969). A major low-level air current near the indian ocean during the northern summer. *Quarterly Journal of the Royal Meteorological Society*, 95(404), 362–380.
- Findlater, J. (1974). The low-level cross-equatorial air current of the western indian ocean during the northern summer. *Weather*, 29(11), 411–416.
- Gebregiorgis, D., Clemens, S. C., Hathorne, E. C., Giosan, L., Thirumalai, K., & Frank, M. (2020). A brief commentary on the interpretation of chinese speleothem  $\delta^{18}\text{O}$  records as summer monsoon intensity tracers. *Quaternary*, 3(1), 7.
- Gebregiorgis, D., Hathorne, E. C., Giosan, L., Clemens, S., Nürnberg, D., & Frank, M. (2018). Southern hemisphere forcing of south asian monsoon precipitation over the past  $\sim$  1 million years. *Nature communications*, 9(1), 1–8.
- Gupta, A. K., Das, M., & Anderson, D. M. (2005). Solar influence on the indian summer monsoon during the holocene. *Geophysical Research Letters*, 32(17).
- Halpern, D., & Woiceshyn, P. M. (2001). Somali jet in the arabian sea, el niño, and india rainfall. *Journal of Climate*, 14(3), 434–441.
- Hurrell, J. W., Holland, M. M., Gent, P. R., Ghan, S., Kay, J. E., Kushner, P. J., ... others (2013). The community earth system model: a framework for collaborative research. *Bulletin of the American Meteorological Society*, 94(9), 1339–1360.
- Jain, S., Mishra, S. K., Anand, A., Salunke, P., & Fasullo, J. T. (2021). Historical and projected low-frequency variability in the somali jet and indian summer monsoon. *Climate Dynamics*, 56(3), 749–765.
- Jalihal, C., Bosmans, J. H. C., Srinivasan, J., & Chakraborty, A. (2019). The response of tropical precipitation to earth’s precession: the role of energy fluxes and vertical stability. *Climate of the Past*, 15(2), 449–462.
- Jalihal, C., Srinivasan, J., & Chakraborty, A. (2019). Modulation of indian monsoon by water vapor and cloud feedback over the past 22,000 years. *Nature communications*, 10(1), 1–8.
- Jalihal, C., Srinivasan, J., & Chakraborty, A. (2020). Different precipitation response over land and ocean to orbital and greenhouse gas forcing. *Scientific reports*, 10(1), 1–11.
- Joseph, P., & Sijikumar, S. (2004). Intraseasonal variability of the low-level jet stream of the asian summer monsoon. *Journal of Climate*, 17(7), 1449–1458.
- Kudrass, H., Hofmann, A., Doose, H., Emeis, K., & Erlenkeuser, H. (2001). Modulation and amplification of climatic changes in the northern hemisphere by the indian summer monsoon during the past 80 ky. *Geology*, 29(1), 63–66.
- Large, W., & Pond, S. (1981). Open ocean momentum flux measurements in moderate to strong winds. *Journal of physical oceanography*, 11(3), 324–336.
- McGrath, S. M., Clemens, S. C., Huang, Y., & Yamamoto, M. (2021). Greenhouse gas and ice volume drive pleistocene indian summer monsoon precipitation isotope variability. *Geophysical Research Letters*, 48(4), e2020GL092249.
- Murtugudde, R., Seager, R., & Thoppil, P. (2007). Arabian sea response to monsoon variations. *Paleoceanography*, 22(4).
- Neale, R. B., Chen, C.-C., Gettelman, A., Lauritzen, P. H., Park, S., Williamson, D. L., ... others (2010). Description of the near community atmosphere model (cam 5.0). *NCAR Tech. Note NCAR/TN-486+ STR*, 1(1), 1–12.
- Pausata, F. S. R., Messori, G., Yun, J., Jalihal, C. A., Bollasina, M. A., & Marchitto, T. M. (2021). The remote response of the south asian monsoon to reduced dust emissions and sahara greening during the middle holocene. *Climate of the Past*, 17(2), 1–30.
- Preethi, B., Mujumdar, M., Kripalani, R., Prabhu, A., & Krishnan, R. (2017).

- Recent trends and tele-connections among south and east asian summer monsoons in a warming environment. *Climate Dynamics*, 48(7-8), 2489–2505.
- Rajendran, K., Kitoh, A., Srinivasan, J., Mizuta, R., & Krishnan, R. (2012). Monsoon circulation interaction with western ghats orography under changing climate. *Theoretical and Applied Climatology*, 110(4), 555–571.
- Reichart, G.-J., Lourens, L., & Zachariasse, W. (1998). Temporal variability in the northern arabian sea oxygen minimum zone (omz) during the last 225,000 years. *Paleoceanography*, 13(6), 607–621.
- Sandeep, S., & Ajayamohan, R. (2015). Poleward shift in indian summer monsoon low level jetstream under global warming. *Climate Dynamics*, 45(1-2), 337–351.
- Sandeep, S., Ajayamohan, R., Boos, W. R., Sabin, T., & Praveen, V. (2018). Decline and poleward shift in indian summer monsoon synoptic activity in a warming climate. *Proceedings of the National Academy of Sciences*, 115(11), 2681–2686.
- Schmiedl, G., & Leuschner, D. C. (2005). Oxygenation changes in the deep western arabian sea during the last 190,000 years: Productivity versus deepwater circulation. *Paleoceanography*, 20(2).
- Tomas, R. A., & Webster, P. J. (1997). The role of inertial instability in determining the location and strength of near-equatorial convection. *Quarterly Journal of the Royal Meteorological Society*, 123(542), 1445–1482.
- Wang, P., Wang, B., Cheng, H., Fasullo, J., Guo, Z., Kiefer, T., & Liu, Z. (2014). The global monsoon across timescales: coherent variability of regional monsoons. *Climate of the Past*, 10(6), 2007–2052.
- Webster, P., Magana, V., Palmer, T., et al. (2003). Dynamical theory. *Encyclopedia of Atmospheric Sciences*, 1370–1385.
- Zhang, H., Ait Brahim, Y., Li, H., Zhao, J., Kathayat, G., Tian, Y., ... others (2019). The asian summer monsoon: Teleconnections and forcing mechanisms—a review from chinese speleothem  $\delta^{18}O$  records. *Quaternary*, 2(3), 26.
- Zhang, H., Cheng, H., Baker, J., & Kathayat, G. (2020). Response to comments by daniel gebregiorgis et al. “a brief commentary on the interpretation of chinese speleothem  $\delta^{18}O$  records as summer monsoon intensity tracers”. *quaternary* 2020, 3, 7. *Quaternary*, 3(1), 8.

# Supporting Information for ”Response of the low-level jet to precession and its implications for proxies of the Indian monsoon”

Chetankumar Jalihal<sup>1,2</sup> \*, Jayaraman Srinivasan<sup>2</sup>, Arindam Chakraborty<sup>1,2</sup>

<sup>1</sup>Centre for Atmospheric and Oceanic Sciences, Indian Institute of Science, Bangalore, 560012, India

<sup>2</sup>DST-Centre of Excellence in Climate Change, Divecha Centre for Climate Change, Indian Institute of Science, Bangalore, 560012,

India

## Contents of this file

1. Figures S1 to S6

---

\*Max Planck Institute for Meteorology,  
Hamburg 20146, Germany

June 8, 2021, 8:49pm

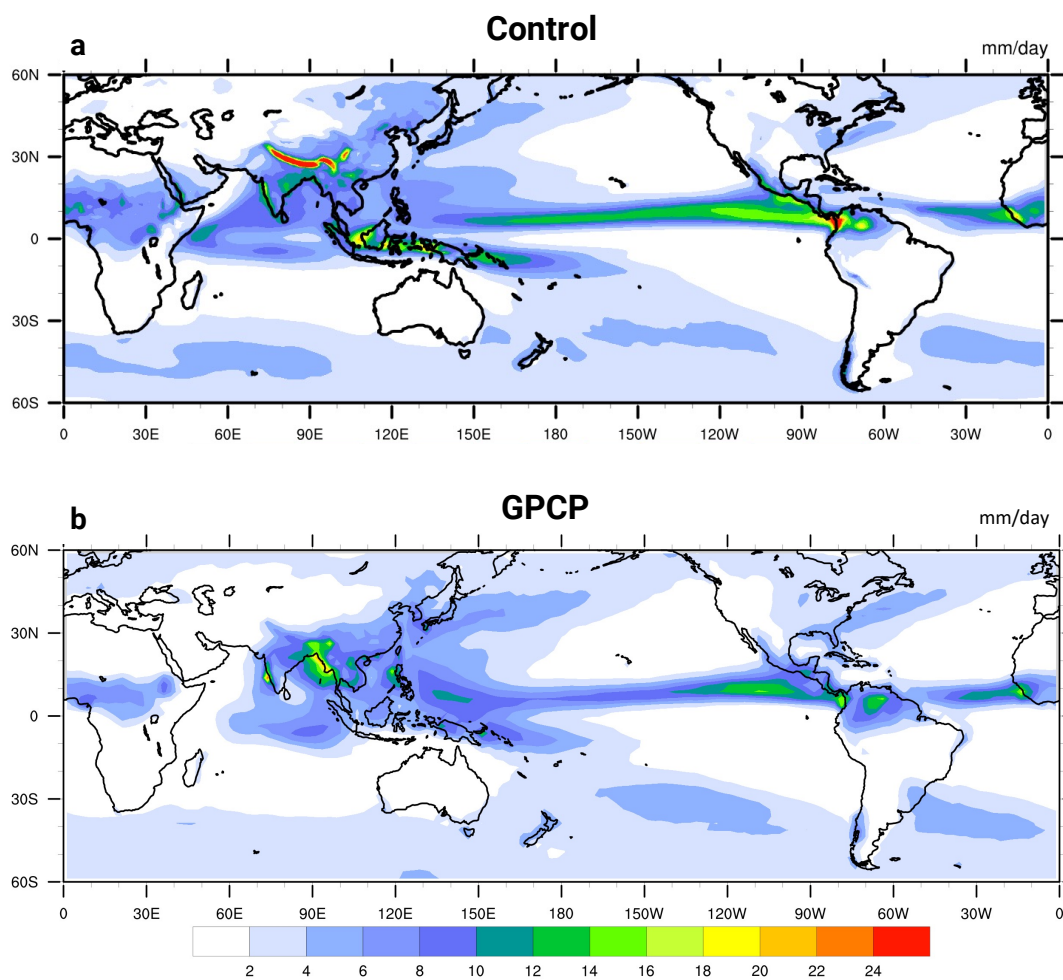


**Figure S1.** The climatological precipitation rate from the (a) pre-industrial control simulation using the fully coupled CESM 1.2.0, and (b) GPCP (Global Precipitation Climatology Project) dataset.

??

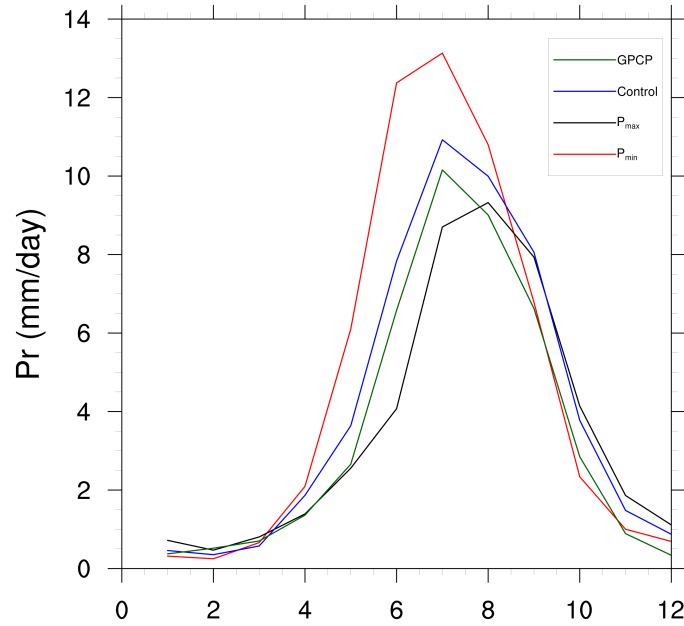


**Figure S2.** The seasonal cycle of precipitation rate, area-averaged over India ( $10^{\circ}\text{N}$ - $29^{\circ}\text{N}$ ,  $73^{\circ}\text{E}$ - $95^{\circ}\text{E}$ ; land only grids), from the pre-industrial control (in blue),  $P_{\min}$  (in red),  $P_{\max}$  (in black), and GPCP (Global Precipitation Climatology Project) data (in green). The control,  $P_{\min}$  (in red), and  $P_{\max}$  are the simulations from the fully coupled CESM 1.2.0. GPCP data over the period 1948–2017 is considered for the climatology.

## CESM 1.2.0; Interannual

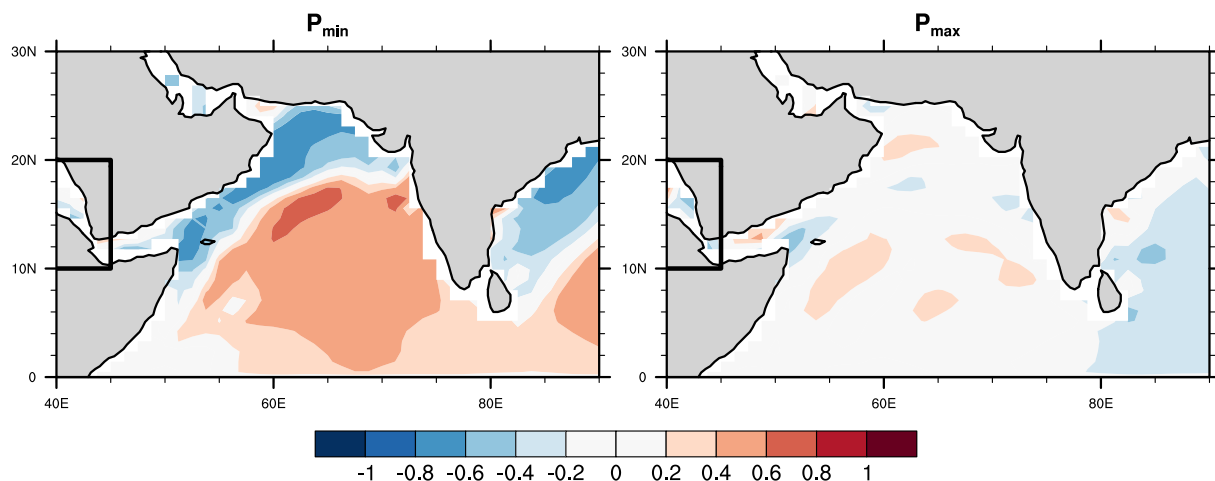


**Figure S3.** The spatial map of correlation between the Jun-Jul-Aug averaged precipitation over northeastern Africa (10°N-20°N, 35°E-45°E) and Ekman upwelling at all the ocean grid points for (a)  $P_{\min}$  (strong monsoon) and (b)  $P_{\max}$  (weak monsoon). The last 50 years of each simulation are considered to evaluate the correlations. Ekman upwelling is calculated based on the curl of wind stress as discussed in the Data and methods section of the main article.

### NCEP (wind speed)

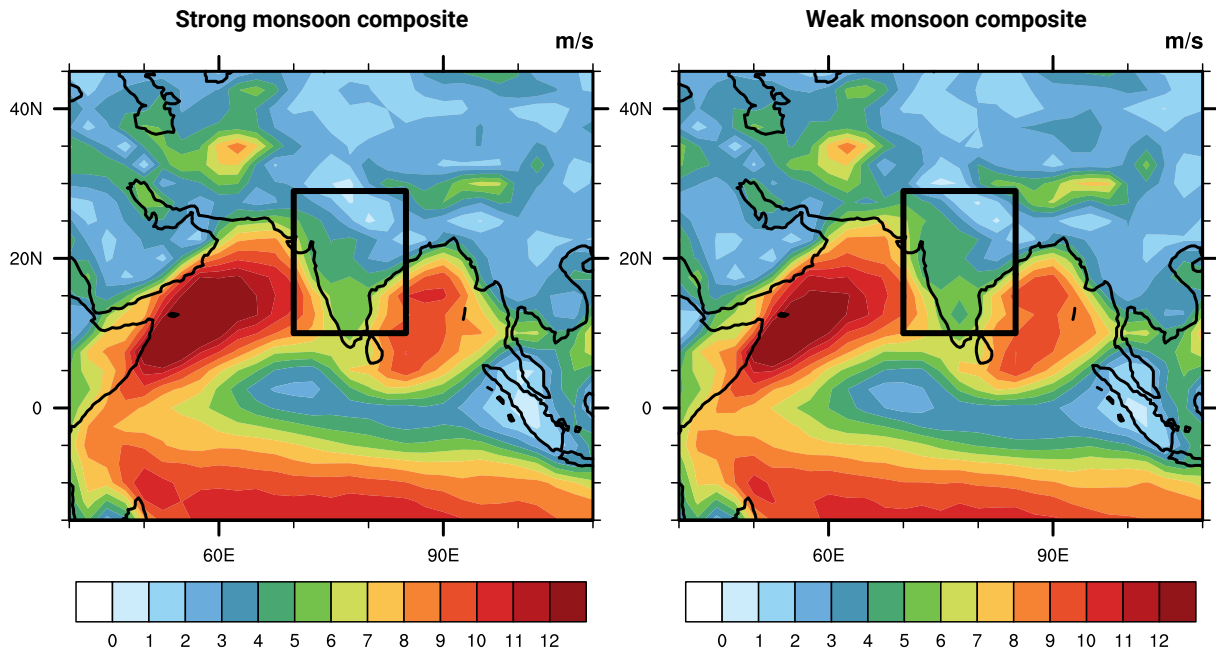


**Figure S4.** The composite of surface wind speed for all the, (a) strong and (b) weak monsoon years from the NCEP reanalysis dataset. Years are classified as strong and weak monsoon years based on the threshold of one standard deviation in all India rainfall about the climatological mean. All India rainfall is the area-averaged precipitation over India ( $10^{\circ}\text{N}$ - $29^{\circ}\text{N}$ ,  $73^{\circ}\text{E}$ - $85^{\circ}\text{E}$ ; land only grids). Precipitation data is taken from GPCP (Global Precipitation Climatology Project). The period 1948–2017 is considered for this analysis.

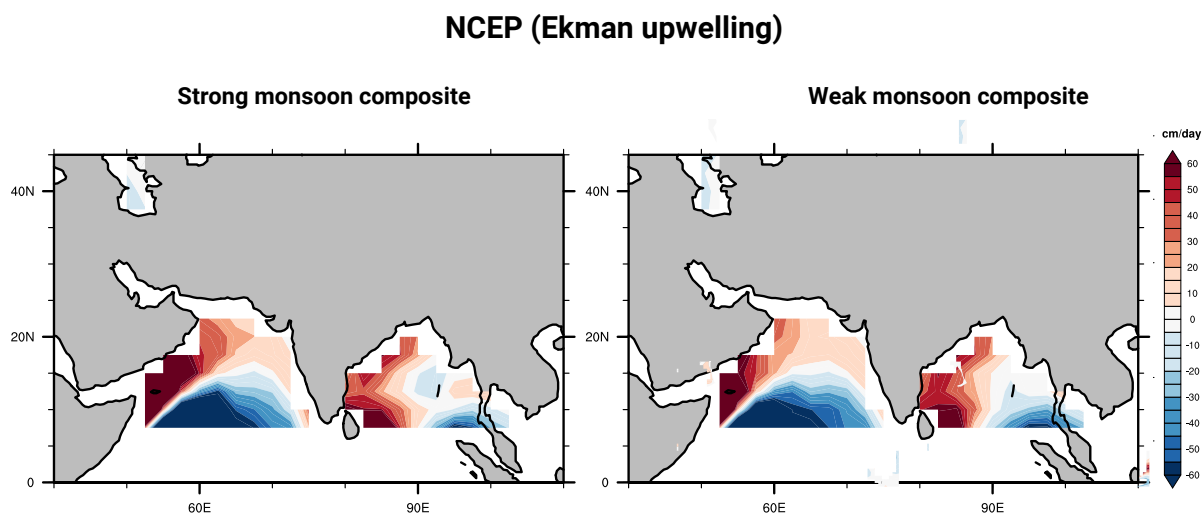


**Figure S5.** The composite of Ekman upwelling for all the, (a) strong and (b) weak monsoon years from the NCEP reanalysis dataset. Years are classified as strong and weak monsoon years based on the threshold of standard deviation in all India rainfall about the climatological mean. All India rainfall is the area-averaged precipitation over India ( $10^{\circ}\text{N}$ - $29^{\circ}\text{N}$ ,  $73^{\circ}\text{E}$ - $85^{\circ}\text{E}$ ; land only grids). Precipitation data is taken from GPCP (Global Precipitation Climatology Project), and Ekman upwelling is evaluated from the surface wind data of NCEP reanalysis as the curl of wind stress. The period 1948–2017 is considered for this analysis.

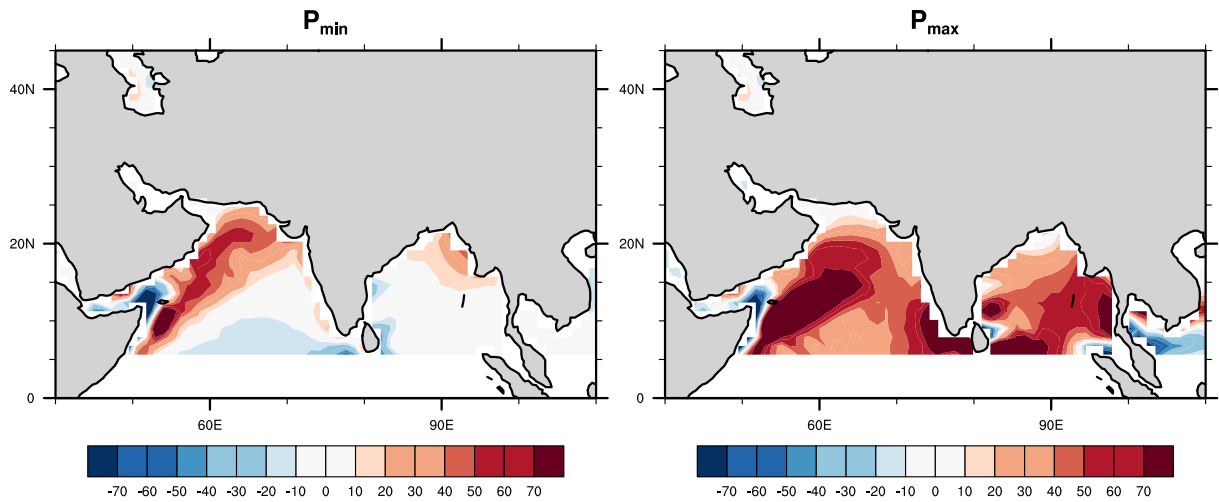


**Figure S6.** The climatological Jun-Jul-Aug averaged Ekman upwelling for (a)  $P_{\min}$  and (b)  $P_{\max}$ . The fully coupled model EC-Earth is used for this analysis (?). Ekman upwelling is calculated based on the curl of wind stress.